

Article

Forming Complex Graded and Homogeneous Components by Joining Simple Presintered Parts of TRIP-Matrix Composite through Powder Forging

Markus Kirschner ^{1,*}, Stefan Martin ², Sergey Guk ¹, Ulrich Prahl ¹ and Rudolf Kawalla ¹

¹ Institute of Metal Forming, Technische Universität Bergakademie Freiberg, 09599 Freiberg, Germany; sergey.guk@imf.tu-freiberg.de (S.G.); ulrich.prahl@imf.tu-freiberg.de (U.P.); rudolf.kawalla@imf.tu-freiberg.de (R.K.)

² Institute of Materials Science, Technische Universität Bergakademie Freiberg, 09599 Freiberg, Germany; stefan.martin@imf.tu-freiberg.de

* Correspondence: markus.kirschner@imf.tu-freiberg.de; Tel.: +49-3731-39-4188

Received: 30 March 2020; Accepted: 17 April 2020; Published: 23 April 2020



Abstract: The ability to fabricate complex graded structures would be a significant step towards the manufacturing of material systems with properties tailored to individual applications. While powder metallurgy has had some success in this regard, it requires that the semi-finished products be exactly similar to the final component. However, it is significantly cheaper to produce simple, semi-finished products and then join them to form complex components with the desired graded structure through powder forging and simultaneous compaction. It is also essential that the graded structure of the semi-finished products is retained during the forming process. In this study, pre-sintered cylindrical semi-finished products consisting of identical homogeneous layers as well as graded components consisting of non-identical homogeneous layers were joined using powder forging at 1100 °C. The microstructures and densities as well as the mechanical properties of the final components were investigated. It was observed that, upon compaction, the components formed solid structures, in which the reinforcing ZrO₂ particles were completely integrated within the transformation-induced plasticity steel matrix. Finally, it was confirmed that the graded structure of the semi-finished products was retained in the final components.

Keywords: powder forging; TRIP-matrix composite; forming; graded structure; homogeneous structure

1. Introduction

Constant progress, particularly in automotive and aerospace technologies and fields such as mechanical and plant engineering, requires materials and components that can withstand ever-increasing loads. The mechanical, tribological, thermal, and chemical stresses involved place exceptionally high demands on the materials used. The development of materials that are based on novel concepts and thus exhibit improved properties tailored to individual applications is one way of solving this problem. This is because this approach allows components to exhibit locally appropriate characteristics. More specifically, functionally graded materials (graded) represent one such option. The aim of research in the field of graded materials is to develop materials wherein constituents with different properties adapted to local requirements are combined in an optimal manner while avoiding interfacial problems [1–3]. Such components may allow for the realization of functional properties not obtainable through direct material transitions [4].

Powder metallurgy is suitable for the production of graded components [4–7]. In general, powder materials can be graded either in layers or in a continuous manner. In the case of graded structures

built up in layers, there is a gradual change in the concentration or material properties within the material system [8,9]. The most commonly used method for the powder metallurgical fabrication of graded materials is layer pressing. In this method, different powder mixtures are filled in the die in a layer-by-layer manner in the corresponding step size, either parallel or perpendicular to the pressing direction. The mixtures are then pressed together and consolidated or sintered [4,6,8–10]. However, a relative density of only approximately 91% can be achieved in this manner. In order to ensure that the density and thus the property profile of the solid component is as desired, a subsequent powder forging step is necessary [10,11]. To ensure a relative density of 100%, the powder forging process of upsetting is used. This involves hot forming with significant lateral material flow. A preform with a simple shape is formed into the more complex shape of the finished part under simultaneous compaction [12–15]. The primary materials used for graded components in powder metallurgy are metals and ceramics [5,16].

Particle-reinforced metal matrix composites represent a predominant part here. Particle-reinforced metal matrix composites exhibit the properties of both the ductile metal matrix and the functional ceramic particles incorporated within the matrix. Hence, they are suitable for use in a range of applications, owing to their higher stiffness, improved strength, which is accompanied by a marginal loss in ductility, and greater wear resistance as compared with those of the unreinforced metal [17–19]. In particular, composites based on high-energy-absorbing transformation-induced plasticity (TRIP)/twinning-induced plasticity steels and transformable zirconia (ZrO_2) particles show great potential [20–23]. For instance, reinforcement with MgO-partially stabilized zirconia (Mg-PSZ) particles can increase the strength as well as the wear properties of these composites, owing to the ability of Mg-PSZ to undergo a stress-induced transformation from the tetragonal phase to the monoclinic phase [24–26]. Furthermore, the use of metastable austenitic steel as the matrix ensures a deformation-induced increase in both the strength and the ductility, owing to the TRIP effect [27,28].

The aim of this study was to experimentally determine the forming conditions for the production of axially formed graded components from a particle-reinforced metal matrix composite using powder forging. The challenge was to ensure that the graded structure was maintained during material cross-flow while simultaneously compacting the components without inducing cracks in the sintered parts or fractures during the forming process.

2. Materials and Methods

The investigated material consisted of a gas-atomized, metastable, high-alloyed Transformation Induced Plasticity (TRIP) steel powder, which was austenitic in structure (with the particle sizes $d_{10} = 8 \mu\text{m}$, $d_{50} = 20 \mu\text{m}$, and $d_{90} = 127 \mu\text{m}$), and a Mg-PSZ ceramic powder (with the particle sizes $d_{10} = 10.6 \mu\text{m}$, $d_{50} = 17.8 \mu\text{m}$, and $d_{90} = 29.6 \mu\text{m}$). The chemical compositions of the TRIP steel (indicated as 16-7-6 TRIP steel) and ZrO_2 ceramic powders are listed in Table 1.

Table 1. Nominal chemical compositions of TRIP steel and Mg-PSZ powders.

TRIP Steel	Fe	C	Cr	Ni	Mn	Si	N	Al	S	Mo	Ti
(wt%)	bal.	0.03	16.3	6.6	7.2	1.0	0.09	0.04	<0.01	<0.01	<0.01
Mg-PSZ	ZrO ₂	HfO ₂	MgO	SiO ₂	Al ₂ O ₃	CaO	TiO ₂	Y ₂ O ₃			
(wt%)	bal.	1.85	3.25	0.1	1.58	0.06	0.13	0.13			

The ceramic particle contents were set to 0 vol% (0%), 5 vol% (5%), 10 vol% (10%), 15 vol% (15%), or 20 vol% (20%). The specimens with a homogenous particle distribution were fabricated by producing a layered structure with one of these five contents, as shown in Figure 1. Then, hot pressing was performed to fabricate a cylinder with a diameter of 80 mm and length of 16.6 mm. Three individual layers were stacked on top of each other before the forming process. This was done to study the interfaces between the layers after powder forging. The target relative density was set to 90% to

simulate the density after sintering in the industry. By the subsequent powder forging, the specimens were compacted to 100% density. On the other hand, the graded specimens were produced by hot pressing layers corresponding to each ZrO_2 content into cylinders with a diameter of 80 mm and length of 10 mm, as shown in Figure 1. The individual layers were stacked on top of each other before the forming process. The relative density of each layer was also set to 90%.

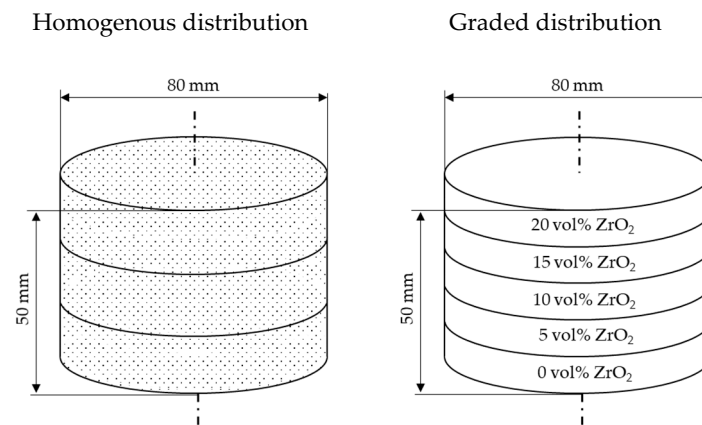


Figure 1. Types of specimens fabricated.

The specimens were formed using a universal forming press at a specimen temperature of 1100 °C (after being heated for 3 h in a protective gas atmosphere to simulate the process after the sintering) and die temperature of 200 °C. This happened in order to simulate the powder forging process in the industry. Boron nitride was used as the lubricant. The holding time was 10 s, and the pressing force was up to 5 MN. The produced component had a cylindrical form with a diameter of 120 mm and length up to 17 mm. A total of five specimens were formed for each condition. The geometry of the die developed for this purpose was derived from model tests performed using the Gleeble HDS-V40 system (Dynamic Systems Inc., Poestenkill, USA) and is shown in Figure 2. Further information can be found elsewhere in the literature [29–32].

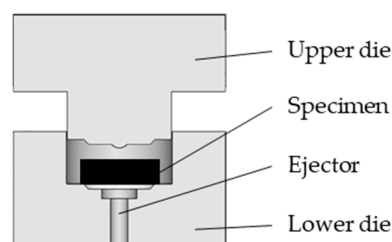


Figure 2. Schematic of the die with the specimen.

The geometry of the specimens was similar to that of a simplified form of a hub. This was done to ensure that the simulated component manufacturing process was as close as possible to the actual one for semi-finished products. The relative density was determined based on hydrostatic weight measurements, which were performed as per the DIN 53217 standard. Mini tensile tests were performed at room temperature as per the DIN EN ISO 6892-1 standard. The test specimens for these tests had a length of 20 mm, width of 7 mm, and thickness of 1 mm, and were taken axially. The repetition frequency was five times per state. Light microscopy images of the specimens were obtained using a VHX-S660E system (Keyence, Neu-Isenburg, Germany), while scanning electron microscopy (SEM) was performed on an Apreo system at 10 kV (Thermo Fisher Scientific, Dreieich, Germany). The microstructures of the specimens, including their phase composition and the characteristics of the zirconia/steel interface, were analyzed through SEM imaging performed on a JEOL JSM 7800F system (JOEL, Freising, Germany) at

2 kV; the SEM system was equipped with an EDAX attachment for energy-dispersive X-ray spectroscopy (EDS, EDAX, Weiterstadt, Germany). For the SEM investigations, the specimens were vibrationally polished on a Buehler Vibromet for 24 h using a colloidal silica suspension. To prevent the accumulation of electrical charge during the SEM investigations, the specimens were coated with a thin carbon layer. Hardness tests were performed on a ZHU250 system (Zwick/Roell, Ulm, Germany) at room temperature as per the DIN EN ISO 6507-4 and DIN EN ISO 6508-1 standards.

3. Results

The semi-finished products were cylindrical with a diameter of 80 mm and length of 50 mm. They were formed in order to investigate the behavior of semi-finished products during forming with simultaneous compaction. Owing to the differences in the ZrO_2 content within the steel matrix for the various specimens, different stress fields would be generated in it. For this reason, the compressive stress applied from the outside had to be large enough to ensure that the hydrostatic and deviating stress components were suitable for achieving full density. Therefore, different compressive forces were necessary for the different ZrO_2 contents, as shown in Figure 3.

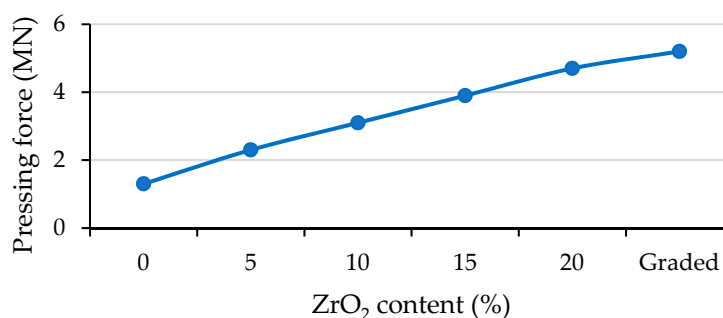


Figure 3. Compressive forces required for different ZrO_2 contents to achieve full density.

It can be seen clearly that the pressing force increased linearly for the ZnO_2 content range of 5–20%. This can be attributed to the reinforcing particles and the stress field generated by them. The specimens without ZrO_2 exhibited a significantly lower pressing force; this can obviously be attributed to the absence of ZrO_2 particles within the matrix. The fact that the specimens with a graded structure required a slightly higher force than those for the specimens in the homogeneous state can be attributed to the differences in the properties and flow conditions of the individual layers. In order to achieve uniform flow and densification, a higher pressing force is required.

Next, semi-finished products after the powder forging are shown in Figure 4.



Figure 4. Specimen with ZrO_2 content of 5%.

It can be seen that the surface of the specimen is heavily scaled. However, this did not pose a problem, since the scale layer flakes off readily with small impacts, resulting in the pure component being exposed. In addition, the tool geometry is well mapped in the component.

These images confirmed that solid components with both homogeneous and graded reinforcing particle distributions can be produced by powder forging. To further verify this, the relative density of each specimen was determined, as shown in Figure 5.

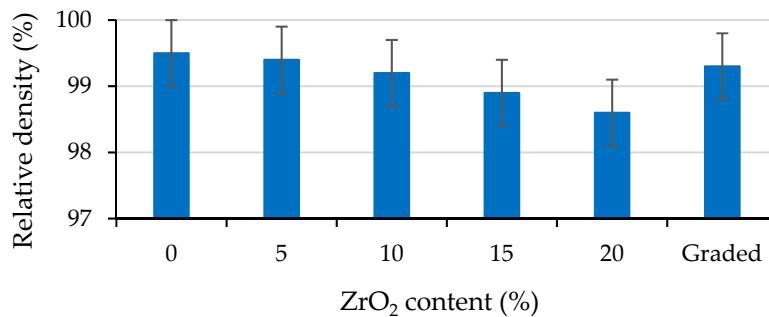


Figure 5. Relative densities of various specimens after the forging process.

It should be noted that the variations in the densities of the graded specimens were not more significant than those in the densities of the specimens with a homogeneous particle distribution. However, despite the measurement error, the specimens with a high ZrO₂ content did not exhibit a relative density of 100%. The reason for this is either the uncertainty in the measurements or the reinforcing particles themselves. The presence of a higher number of reinforcing particles increases the probability of cluster formation. One such cluster is displayed in Figure 6. It can be seen clearly how one of the reinforcing particles is exposed and has a large pore around it while the other exposed particles are completely enclosed within the matrix.

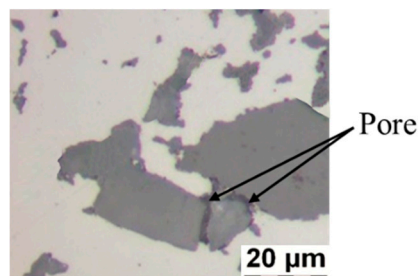


Figure 6. Pores generated within the matrix of the 20% ZrO₂ specimen owing to particle cluster formation.

To analyze the microstructures of the various specimens, light microscopy images of their sections were taken, as shown in Figure 7. It can be clearly seen that, in the homogeneous specimen, the reinforcing particles remain distributed randomly and do not show significant clustering. However, aligned particles can be seen in Figure 7d. This alignment of the particles can be attributed to the fact that the particles followed the material flow of the matrix. As evidenced by the high density of the specimen (see Figure 5), the particles were completely integrated within the matrix, and only a few pores were formed, either at or near the interface, as shown in Figure 7a. The gradient in the ZrO₂ volume fraction was retained during the forming process, as shown in Figure 7c. The gradient can be seen in the outer area of the specimen where an expansion of the individual ZrO₂ content, in comparison to the specimen core, is visible. This can, however, be attributed to the flow of the material during the forming process. In addition, neither delamination nor cracks were observed between the individual layers, as is evident from Figure 7b,d.

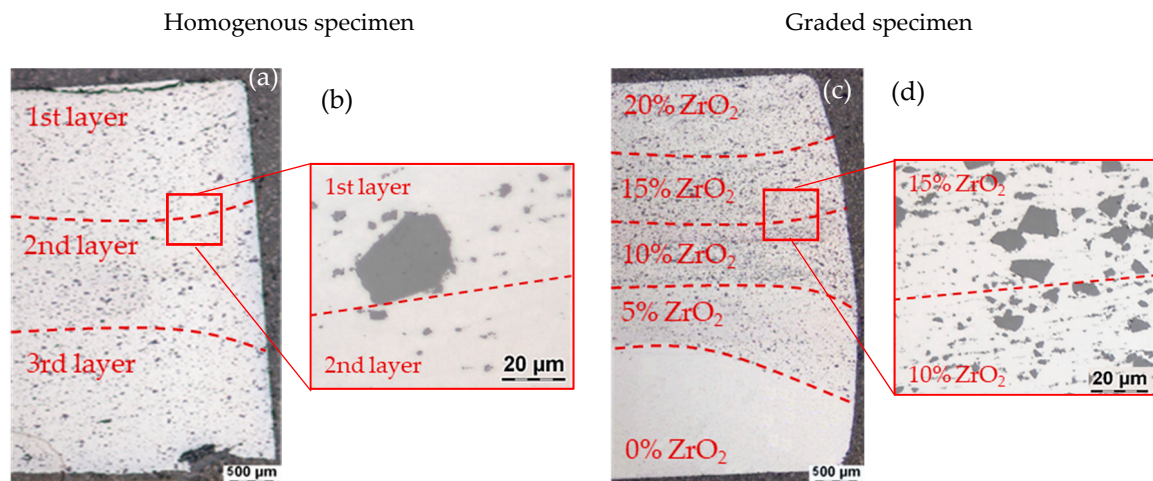


Figure 7. Specimens obtained after subjecting pre-sintered specimens to the forming process: (a) overview of homogenous specimen with 10% ZrO_2 , (b) boundary between two layers with ZrO_2 content of 10%, (c) overview of graded specimen, and (d) boundary between layers with ZrO_2 contents of 10% and 15%.

In order to evaluate the interfaces in greater detail and analyze the interfacial reactions, SEM analysis was performed. At the interfaces between the layers, no microcracks were observed. Only fine oxide particles with necklace-like structures were seen, as shown in Figure 8a. Figure 8c shows that the ZrO_2 particles were embedded within the steel matrix. The contrast of the backscattered electrons image was chosen such that the differences in the orientations of the particles and the steel matrix could be visualized with ease. The steel matrix had an austenitic microstructure and did not undergo a martensitic transformation during the hot-forging process and the subsequent cooling to room temperature. It should be noted that the dark areas and spots in the image are not pores. In fact, these areas would look like the interfaces shown in Figure 8b if the greyscale distribution of the image were to be optimized for these phases. However, in order to highlight the orientations of the dominant phases, these oxide phases are shown in black owing to their low backscatter coefficient. This, in turn, is attributable to the lower average atomic number of the compound. Within the zirconia particles, the black spots are mainly MgO , which is precipitated at the internal interfaces as reported elsewhere [33]. Furthermore, only a small monoclinic phase fraction is visible in the particles (see Figure 8b,c), because the monoclinic phase appears brighter in the image than the initial phase. This is owing to the diffusion of MgO , which destabilizes ZrO_2 . ZrO_2 has a higher effective atomic number without Mg as a stabiliser and thus appears brighter in the image than the initial phase.

Along the steel/ceramic interface, two distinct EDS line scans were performed, as shown in Figure 9a,b. Along line scan 1, an interface without a reaction layer was observed. The slope of the change in the concentrations of the elements at the interface of the composite constituents in Figure 9a is related to the inclination of the interface below the observational plane of the specimen. Moreover, an interface without a reaction layer is shown in Figure 8d. It can be assumed that the interdiffusion of the constituent elements did not occur, given that, at these temperatures, Mg does not dissolve in face-centered cubic austenite and that Mn could be solved in cubic zirconia only at higher temperatures above $1400\text{ }^\circ\text{C}$. A newly formed phase at the interface in the line scan (see Figure 9b) shows clearly the interdiffusion of Mn and Mg from both sides into the reaction layer. This phase is probably related to $(Mg_{1-x}, Mn_x)_2SiO_4$, which exhibits complete miscibility between Mg_2SiO_4 and Mn_2SiO_4 . Owing to the interdiffusion of Mn and Mg into the interfacial phase, it can be expected that there is a strong connection between the individual phases constituents of the composite.

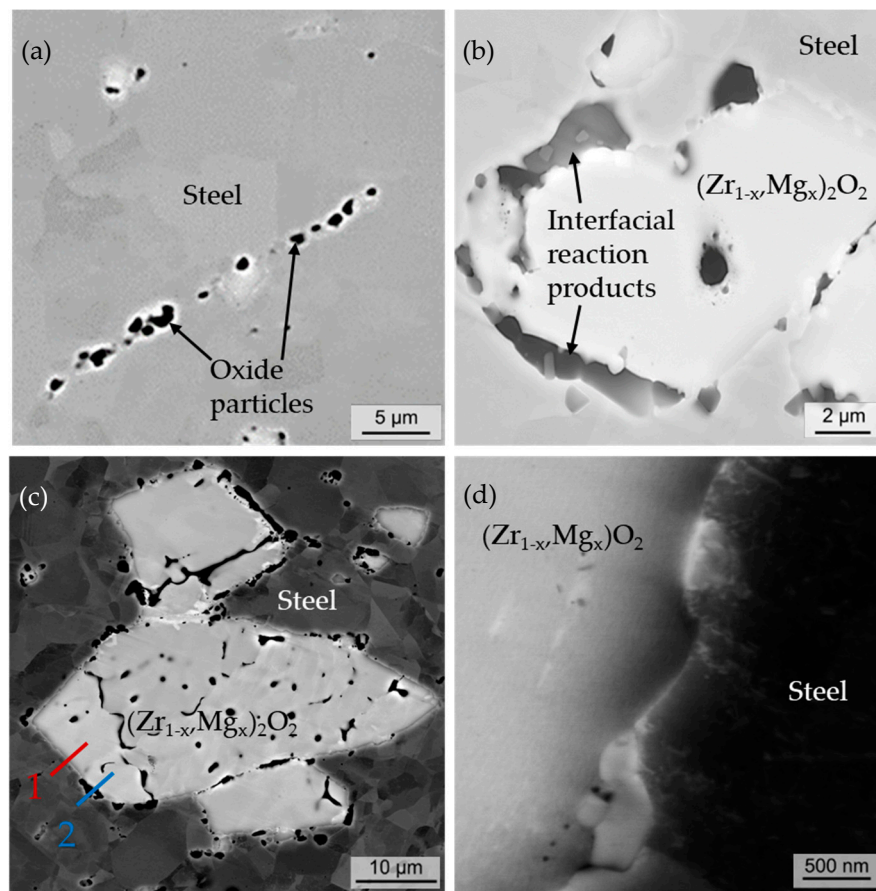


Figure 8. SEM images based on backscattered electrons: (a) necklace-like oxide particles (magnification: 1000×), (b) zirconia particle with distinct reaction layer at interface with steel matrix (magnification: 5000×), (c) characteristic microstructure of composite (two EDS line scans across interface are highlighted; magnification: 1500×), and (d) interface without reaction layer; dislocations are visible next to interface of composite (magnification: 25,000×).

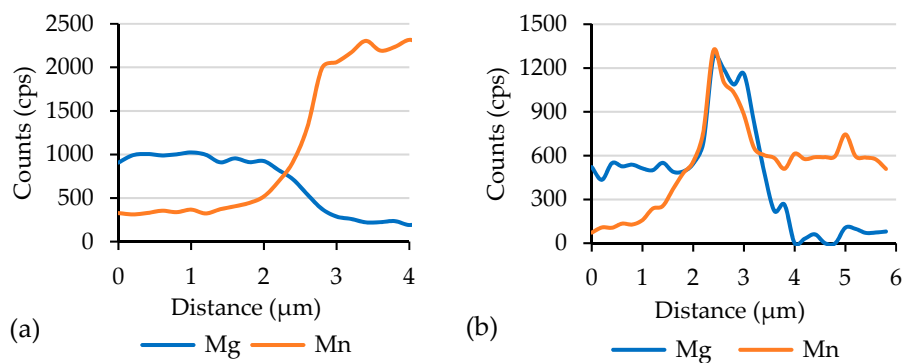


Figure 9. EDS line scans shown in Figure 8c: (a) EDS line scan 1 and (b) EDS line scan 2.

On observing the tensile test specimens, it can be seen that the homogeneous specimens broke almost in the middle, while the graded specimens broke at one of the head ends (see Figure 10); the head end had the highest content of ZrO_2 —20%. However, all specimens exhibited a fracture angle of approximately 45° .

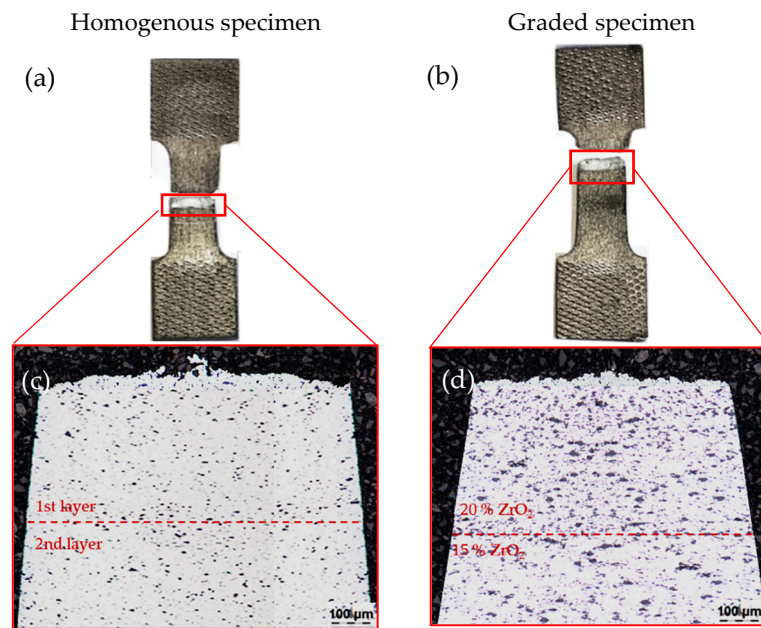


Figure 10. Tensile test specimens with (a) homogeneous and (b) graded particle distributions and (c,d) light microscopy images of their meridian sections.

This fracture behavior was also evident from the results of the tensile tests, which are listed in Table 2. The tensile stress increased with increase in the proportion of the reinforcing particles. This can be attributed to the reinforcement effect of the particles. It can also be seen that the graded specimens exhibited a higher strain than those of the homogenous specimens with 15% and 20% ZrO_2 . Moreover, the latter specimens showed lower strains. In addition, these specimens did exhibit a decrease in yield strength and underwent brittle fractures.

Table 2. Changes in mechanical properties with ZrO_2 content.

ZrO_2 Content (%)	Tensile Yield Strength (MPa)	Ultimate Tensile Strength (MPa)	Fracture Strain (%)
0	304	959	39
5	393	951	36
10	469	948	35
15	518	875	26
20	577	858	16
Graded	442	894	28

Both the Vickers hardness and Rockwell hardness values are plotted in Figure 11. It can be seen that the hardness increased with the content of reinforcing particles. It is also evident that there were no differences between the curves for the Rockwell and Vickers hardnesses, with the curves exhibiting the same gradient.

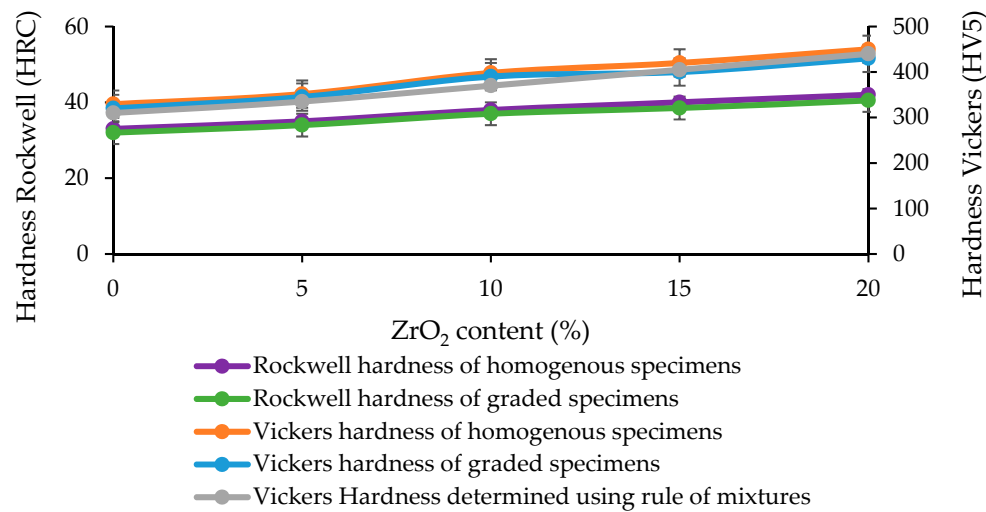


Figure 11. Vickers and Rockwell hardnesses of homogeneous specimens with different ZrO₂ contents and those of graded specimens.

However, it can also be seen that, in the case of the graded specimens with ZrO₂ contents of 10% and higher, the hardness curves did not follow those of the homogeneous specimens but are slightly lower. Furthermore, it can be stated that the measured hardness values are verified, since they agree with each other and the calculated hardness for Vickers based on the rule of mixtures.

Therefore, the graded specimens did not exhibit tensile strengths as high as those of the homogeneous specimens, which also showed higher strains. It is possible to calculate the tensile strength of a material from its hardness [34,35]. Thus, it can be seen clearly from Figure 12 that the curve for the calculated tensile strength is the same as that for the measured tensile strength. However, in the case of the specimen with a ZrO₂ content of 15%, the curves do not match.

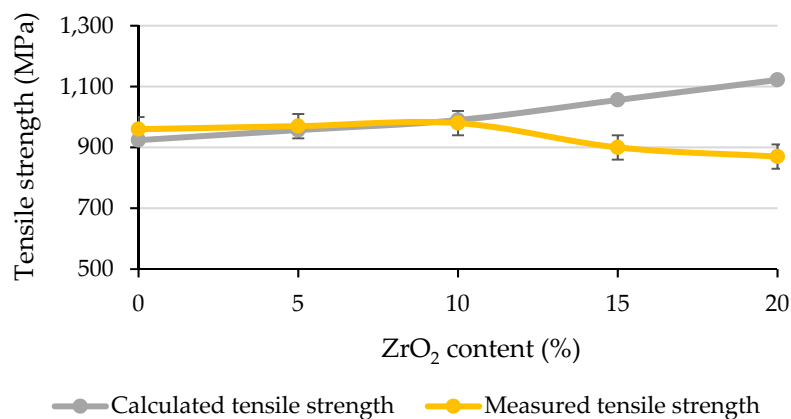


Figure 12. Calculated and measured tensile strengths for different ZrO₂ contents.

4. Discussion

4.1. Light Microscopy Imaging

The presence of clusters in Figure 6 can be explained as follows. While smaller clusters can be dissolved by the material flow that occurs within the matrix, this flow may not be strong enough to break the larger clusters completely. These clusters increase the stress in the matrix locally. This phenomenon is the opposite of material flow, which is essential for the compaction and integration of the particles into the matrix. Thus, the material flow in the clusters may even come to a complete

halt [36,37]. This meant that complete compaction in this area was no longer possible, because of which the specimens with a ZrO_2 content of 20% did not exhibit the desired relative density (see Figure 5).

4.2. SEM Imaging

The presence of oxides in Figure 8 can be explained as follows. These oxides are formed from the initial native oxides present on the surfaces of the steel powder particles. The oxides are mainly manganese silicates (Mn_2SiO_4), because interfacial reactions occur between the steel matrix and the ZrO_2 particles, and several compounds are formed, as shown in Figure 8b [38]. The main elements involved in these reactions are Mn, Cr, and Si from the steel matrix and MgO from the zirconia particles. As the partially stabilized zirconia is subjected to forging at 1100 °C in the phase field of tetragonal ZrO_2 and MgO [39], the zirconia solid solution decomposes, and the MgO diffuses to the interface. Further, Al_2O_3 impurities from the ZrO_2 powder also participate in the reaction. Because of this destabilization process, only small monoclinic zirconia crystallites are formed at the edges of the reinforcing zirconia particles, and the rest of the particles remain in the initial phase [40]. This means that the transformation of the reinforcing ZrO_2 phase and the TRIP effect, which is attributable to the austenitic microstructure—a primary characteristic of TRIP-matrix composites—are maintained even after the powder forging process.

4.3. Tensile Tests

The reason the graded specimens broke at one of the head ends during the tensile tests was also particle distribution. The area with a high ZrO_2 content was located in this part of the specimens, as can be seen from the meridian sections of the specimens. It can also be seen that the homogeneous specimens did not crack at the interfaces between the individual layers. This was also true for the graded specimens, in which cracks formed above the phase boundary between the 15% and 20% ZrO_2 layers. These cracks clearly migrated through the matrix. Therefore, failure at these points was caused by the pores remaining in the clusters, as discussed above. These pores act as crack initiation sites owing to the notch effect [41,42]. More specifically, these cracks extend from one reinforcing particle to the next, as described in the literature [43–47]. Thus, the cracks in the matrix spread rapidly, even though the distance between the reinforcing particles is small [43,45,47]. This is the reason brittle fracturing was observed with an increase in the ZrO_2 content. This can be confirmed from the image given in Figure 13, which shows the propagation path of a crack in the layer with a ZrO_2 content of 15%.

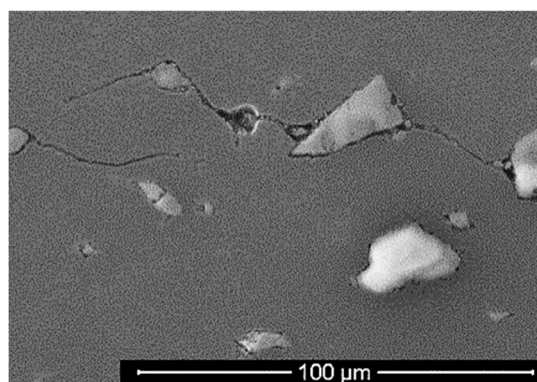


Figure 13. Crack propagation in the homogenous specimen matrix (magnification: 1500×).

However, crack initiation and propagation did not occur more frequently in the layer boundaries, and the cracks formed randomly in the matrix of the specimens. Thus, it can be concluded that the forming joints did not serve as crack initiation points.

The differences in the strain values of the graded and homogeneous specimens with the highest ZrO_2 content can be attributed to the differences in the strain distributions within the specimens.

Because the ZrO₂-poor layers deform more readily than the ZrO₂-rich ones, most of the stress is absorbed in the former. Thus, crack initiation and propagation in the ZrO₂-rich layers does not start immediately, in contrast to the case for the homogeneous specimens, since the stress required for this is absorbed by the ZrO₂-poor layers. Thus, cracks are only initiated when the stress is high enough to deform the layers with high ZrO₂ contents. This leads to a higher strain on the specimen itself, as can be seen in Figure 10.

Further, it can be seen clearly from Figure 12 that the curve for the theoretical tensile strength, calculated from hardness, is the same as that for the measured tensile strength. Only for ZrO₂ contents of 15 and higher do the curves not match. This is because of the lower strain and brittle fracturing of the specimens with 15% and 20% ZrO₂ [48]. These two factors, in turn, are attributable to the phenomenon of crack initiation described above.

4.4. Hardness Tests

The observed increase in the hardness with the ZrO₂ content can be explained by the fact that the reinforcing particles counteract the deformation induced during the hardness test. It should also be noted that the hardness values of TRIP steels are high because of the martensitic transformation during plastic deformation, which is dedicated the TRIP effect. During the hardness measurements, a stress is introduced within the microstructure, which triggers the TRIP effect. This was confirmed by the hardness values determined based on the rule of mixtures. Here, the pure hardness values of the martensite and ZrO₂ phases were assumed, and it was found that the calculated values matched the measured ones. Therefore, the hardness tests measured the martensite hardness of the TRIP steel.

The fact that the hardness values calculated based on the rule of mixtures at low ZrO₂ contents were highly consistent with the measured ones also meant that the residual pores present within the material no longer had a determining effect on the properties of the components. Otherwise, the theoretical hardness values would have been higher than the measured ones, since the remaining pores would have adversely affected the component properties, as reported previously [49].

However, it can be seen that the graded specimens with ZrO₂ contents of 10% and higher did not exhibit the same hardness values as those of the homogeneous specimens. In fact, the values of the former were slightly lower. This can be explained by the compaction of the graded components. The reinforcing particles induce a stress field that is the opposite of the stress field of the external force. Thus, the layers with a high ZrO₂ content are compressed to a smaller degree than those with a low ZrO₂ content. This is also reflected in the density distribution given in Figure 5, which shows that the density is lower at high ZrO₂ contents. This, in turn, leads to a lower hardness, as also reported in a previous study [29]. Finally, it should also be noted that the calculated hardness values indicate that graded TRIP matrix composites would be a suitable material for gears, which would not have to be nitrided at great expense.

5. Conclusions

In this study, we hot-formed simple semi-finished products of a TRIP matrix composite at 1100 °C into complex components with the desired graded structure, while simultaneously performing compaction. This was accomplished using a powder forging process. The main conclusions of the study can be summarized as follows:

(1) It is possible to compress individual pre-sintered specimens with a homogeneous reinforcing particle distribution into specimens with a homogeneous and also with an axially graded particle distribution through a forming process and at the same time to obtain a local homogeneous particle distribution.

(2) With an increase in the content of the reinforcing particles, the specimens could be compacted completely or almost completely.

(3) In both the homogenous specimens and the graded ones, the reinforcing particles were completely incorporated within the TRIP steel matrix, resulting in a solid compound consisting of the matrix as well as the particles.

(4) No phase boundaries were visible in the matrix between the individual pre-sintered specimens that had been formed and compacted into a single component.

(5) The phases with high particle contents were the weakest parts of the graded specimens, owing to the presence of crack initiation sites in these phases, which facilitated crack propagation.

(6) The yield strength increased with an increase in the ZrO₂ content. Further, specimens with ZrO₂ contents of 15% and higher exhibited brittle fracture behavior and low strain at break values. This was owing to the notch effect of the residual pores on the reinforcing particles as well as crack propagation owing to the reinforcing particles.

(7) The measured hardness values corresponded to the measured tensile strength values as well as the calculated hardness values. The specimens with ZrO₂ contents higher than 10% exhibited lower hardness values than those calculated. This was attributable to the density of the specimens.

(8) In the homogeneous specimens, an increase in the ZrO₂ content resulted in small remaining residual pores. However, these became crack initiation sites.

(9) The potential TRIP effect by remaining austenitic in the steel matrix as well as the tetragonal structure of ZrO₂ was retained even after the powder forging and forming processes. Thus, the premature phase transformations that do not occur during the manufacturing process do not adversely affect the properties of the components.

Author Contributions: Conceptualization, M.K.; methodology, M.K. and S.G.; formal analysis, M.K.; investigation, M.K. and S.M.; writing—original draft preparation, M.K. (except part SEM) and S.M. (part SEM); writing—review and editing, S.M., S.G. and U.P.; visualization, M.K. and S.M.; supervision, S.G., U.P.; project administration, S.G. and R.K.; funding acquisition, R.K. and S.G. All authors have read and agreed to the published version of the manuscript.

Funding: This work was financed by the German Research Foundation (Deutsche Forschungsgemeinschaft or DFG) and was a part of the Collaborative Research Center TRIP-Matrix-Composites (SFB 799) Subproject A6 I.

Acknowledgments: We thank the Fraunhofer Institute for Ceramic Technologies and Systems in Dresden for assistance with production of the semi-finished specimens.

Conflicts of Interest: The authors declare no conflict of interest.

References

- Liew, K.M.; Lei, Z.; Zhang, L.W. Mechanical analysis of functionally graded carbon nanotube reinforced composites: A review. *Compos. Struct.* **2015**, *120*, 90–97. [[CrossRef](#)]
- Pourmajidian, M.; Akhlaghi, F. Fabrication and Characterization of Functionally Graded Al/SiCp Composites Produced by Remelting and Sedimentation Process. *J. Mater. Eng. Perform.* **2014**, *23*, 444–450. [[CrossRef](#)]
- Birman, V.; Byrd, L.W. Modeling and Analysis of Functionally Graded Materials and Structures. *Appl. Mech. Rev.* **2007**, *60*, 195–216. [[CrossRef](#)]
- Raßbach, S. Grundlegende Untersuchungen zum Umformverhalten von Gradientenwerkstoffen unter Anwendung von Druckformverfahren. PhD Thesis, TU Bergakademie Freiberg, Freiberg, Saxony, 2002.
- Elsner, P. Gradierte Werkstoffeigenschaften: Eine Herausforderung für die Fertigungstechnik. *Futur* **2005**, *14*, 16–18.
- Behrens, B.-A.; Vahed, N.; Brand, H. (Eds.) *Pulvermetallurgische Herstellung Gradiertes Werkzeugwerkstoffe*, 1st ed.; Leibniz Universität Hannover: Hannover, Germany, 2013.
- Kolaska, H. (Ed.) *Fortschritte bei der Formgebung in Pulvermetallurgie und Keramik: Vorträge anlässlich des Symposiums am 28.29. November 1991 in Hagen*; Verband Deutscher Ingenieure: Düsseldorf, Germany, 1991.
- Li, J.; Sun, W.; Ao, W.; Gu, K.; Xiao, P. Al₂O₃-FeCrAl composites and functionally graded materials fabricated by reactive hot pressing. *Compos. Part A* **2007**, *28*, 615–620. [[CrossRef](#)]
- He, Z.; Ma, J.; Tan, G. Fabrication and characteristics of alumina-iron functionally graded materials. *J. Alloy. Compd.* **2009**, *486*, 815–818. [[CrossRef](#)]

10. Sahu, M.; Dargar, M.K.; Bartaria, V.N. The Effect of hot forging and heat treatment on tribological properties of Al alloy & nano composites. *Int. J. Sci. Eng. Technol.* **2013**, *62*, 649–661.
11. Schiller, W. Neue Konzepte zum Kalibrieren von Sinterbauteilen. Master Thesis, Montanuniversität Leoben, Leoben, Austria, 2010.
12. Zapf, G. *Handbuch der Fertigungstechnik: Urformen*; Carl Hanser Verlag: München, Germany, 1981.
13. Vossen, K. Pulverschmieden von gerad- und schrägverzahnten Zylinderrädern. PhD Thesis, RWTH Aachen, Aachen, Germany, 1987.
14. Kuhn, H.A.; Lynn, B. Powder forging. *Powder Metall.* **1990**, *12*, 13–19.
15. Exner, H.E.; Danninger, H. *Handbook of Inorganic Chemistry, Metallurgy of Iron: Powder Metallurgy of Steel*, 10th ed.; Springer: Berlin/Heidelberg, Germany, 1992.
16. Gillia, O.; Caillens, B. Fabrication of a material with composition gradient for metal/ceramic assembly. *Powder Technol.* **2011**, *208*, 355–366. [[CrossRef](#)]
17. Chawla, N.; Shen, Y.-L. Mechanical Behavior of Particle Reinforced Metal Matrix Composites. *Adv. Eng. Mater.* **2001**, *6*, 357–370. [[CrossRef](#)]
18. Kaczmar, J.; Pietrzak, K.; Włosiński, W. The production and application of metal matrix composite materials. *J. Mater. Process. Technol.* **2000**, *106*, 58–67. [[CrossRef](#)]
19. Miracle, D. Metal matrix composites—From science to technological significance. *Compos. Sci. Technol.* **2005**, *65*, 2526–2540. [[CrossRef](#)]
20. Biermann, H.; Aneziris, C.G.; Kolbe, A.; Martín, U.; Müller, A.; Schärfl, W.; Herrmann, M. Microstructure and compression strength of novel TRIP-steel/Mg-PSZ composites. *Adv. Eng. Mater.* **2010**, *12*, 1000–1006. [[CrossRef](#)]
21. Glage, A.; Weigelt, C.; Räthel, J.; Biermann, H. Fatigue behaviour of hot pressed austenitic TWIP steel and TWIP steel/Mg-PSZ composite materials. *Int. J. Fatigue* **2014**, *65*, 9–17. [[CrossRef](#)]
22. Ehinger, D.; Krüger, L.; Martin, U.; Weigelt, C.; Aneziris, C. Buckling and crush resistance of high-density TRIP-steel and TRIP-matrix composite honeycombs to out-of-plane compressive load. *Int. J. Solids Struct.* **2015**, *66*, 207–217. [[CrossRef](#)]
23. Weigelt, C.; Jahn, E.; Berek, H.; Aneziris, C.G.; Eckner, R.; Krüger, L. Joining of Zirconia Reinforced Metal-Matrix Composites by a Ceramics-Derived Technology. *Adv. Eng. Mater.* **2015**, *17*, 1357–1364. [[CrossRef](#)]
24. Zhou, Y.; Guo, Y.; Li, D. Effects of load mode on mechanical properties of ZrO₂ (2Y)/TRIP steel composites. *Trans. Nonferrous Met. Soc. China* **2003**, *13*, 1086–1091.
25. Guo, Y.; Zhou, Y.; Li, D. Microstructure and performance of 2Y-PSZ/TRIP steel composites. *J. Mater. Sci. Technol.* **2003**, *19*, 137–140.
26. Weigelt, C.; Aneziris, C.; Ehinger, D.; Eckner, R.; Krüger, L.; Ullrich, C.; Rafaja, D. Effect of zirconia and aluminium titanate on the mechanical properties of transformation-induced plasticity-matrix composite materials. *J. Compos. Mater.* **2015**, *49*, 3567–3579. [[CrossRef](#)]
27. Zackay, V.F.; Parker, E.R.; Fahr, D.; Busch, R. The enhancement of ductility in high-strength steels. *Trans. Am. Soc.* **1967**, *60*, 252–259.
28. Tamura, I. Deformation-induced martensitic transformation and transformation-induced plasticity in steels. *Met. Sci.* **2013**, *5*, 245–253. [[CrossRef](#)]
29. Kirschner, M. *Beitrag zur Bewertung des Verdichtungsgrades mittels Visioplatsizität*; Werkstoffwoche: Dresden, Germany, 2019.
30. Kirschner, M.; Eckner, R.; Guk, S.; Krüger, L.; Kawalla, R.; Prahl, U. Deformation Behavior of Particle Reinforced TRIP Steel/MgPSZ Composite at Hot Working Temperatures. *Steel Res. Int.* **2019**, *90*, 1800334. [[CrossRef](#)]
31. Kirschner, M.; Guk, S.; Kawalla, R.; Prahl, U. Further Development of Process Maps for TRIP Matrix Composites during Powder Forging. *Mater. Sci. Forum* **2019**, *949*, 15–23. [[CrossRef](#)]
32. Biermann, H.; Aneziris, C.G. (Eds.) *Austenitic TRIP/TWIP Steels and Steel-Zirconia Composites: Powder Forging of pre-sintered TRIP-Matrix Composites*. (M. Kirschner, S. Guk, R. Kawalla, U. Prahl); Springer Series in Materials Science 298; Springer: Berlin/Heidelberg, Germany, 2020; Volume 1.
33. Martin, S.; Berek, H.; Aneziris, C.G.; Martin, U.; Rafaja, D. Pitfalls of local and quantitative phase analysis in partially stabilized zirconia. *J. Appl. Crystallogr.* **2012**, *45*, 1136–1144. [[CrossRef](#)]
34. Deutsches Institut für Normung. *Bibl* **1976**, *10*. [[CrossRef](#)]

35. Meyer, R.J.; Pietsch, E. (Eds.) *Eisen-Härteprüfverfahren: Beziehung zwischen Härte und Zugfestigkeit, Achte Völlig neu Bearbeitete Auflage. Fe. Eisen. Iron (System-Nr. 59), F-e/C/I*; Springer: Berlin/Heidelberg, Germany, 1974.
36. Pranke, K.; Guk, S. Material Flow in Mg-PSZ Particle Reinforced TRIP-Matrix-Composites due to Hot-Rolling. *Key Eng. Mater.* **2016**, *684*, 97–103. [[CrossRef](#)]
37. Guk, S.; Pranke, K.; Müller, W. Flow Curve Modelling of an Mg-PSZ Reinforced TRIP-matrix-composite. *ISIJ Int.* **2014**, *54*, 2416–2420. [[CrossRef](#)]
38. Berek, H.; Yanina, A.; Weigelt, C.; Aneziris, C.G. Determination of the Phase Distribution in Sintered TRIP-Matrix/Mg-PSZ Composites using EBSD. *Steel Res. Int.* **2011**, *82*, 1094–1100. [[CrossRef](#)]
39. Pavlyuchkov, D.; Dilner, D.; Savinykh, G.; Fabrichnaya, O. Phase Equilibria in the ZrO₂-MgO-MnO_x System. *J. Am. Ceram. Soc.* **2016**, *99*, 3136–3145. [[CrossRef](#)]
40. Martin, S.; Decker, S.; Krüger, L.; Martin, U.; Rafaja, D. Microstructure Changes in TRIP Steel/Mg-PSZ Composites Induced by Low Compressive Deformation. *Adv. Eng. Mater.* **2013**, *15*, 600–608. [[CrossRef](#)]
41. Bokuchava, G.; Gorshkova, Y.; Papushkin, I.V.; Guk, S.V.; Kawalla, R. Investigation of Plastically Deformed TRIP-Composites by Neutron Diffraction and Small-Angle Neutron Scattering Methods. *J. Surf. Investig. X-ray Synchrotron Neutron Tech.* **2018**, *12*, 227–232. [[CrossRef](#)]
42. Guk, S.; Milisova, D.; Pranke, K. Influence of Deformation Conditions on the Microstructure and Formability of Sintered Mg-PSZ Reinforced TRIP-Matrix-Composites. *Key Eng. Mater.* **2016**, *684*, 86–96. [[CrossRef](#)]
43. Li, C.; Ellyin, F. Short crack growth behavior in a particulate-reinforced aluminum alloy composite. *Met. Mater. Trans. A* **1995**, *26*, 3177–3182. [[CrossRef](#)]
44. Hochreiter, E.; Panzenböck, M.; Jeglitsch, F. Fatigue properties of particle-reinforced metal-matrix composites. *Int. J. Fatigue* **1993**, *15*, 493–499. [[CrossRef](#)]
45. Seo, B.H.; Kim, J.; Park, J.B.; Jung, G.D. Crack propagation characteristics of particulate reinforced composites using digital image correlation. *Mater. und Werkst.* **2015**, *46*, 387–393. [[CrossRef](#)]
46. Shang, J.K.; Ritchie, R. On the particle-size dependence of fatigue-crack propagation thresholds in SiC-particulate-reinforced aluminum-alloy composites: Role of crack closure and crack trapping. *Acta Met.* **1989**, *37*, 2267–2278. [[CrossRef](#)]
47. Wang, Z.; Zhang, R.J. Microscopic characteristics of fatigue crack propagation in aluminum alloy based particulate reinforced metal matrix composites. *Acta Met. et Mater.* **1994**, *42*, 1433–1445. [[CrossRef](#)]
48. Guk, S.; Müller, W.; Pranke, K.; Kawalla, R. Mechanical Behaviour Modelling of an Mg-Stabilized Zirconia Reinforced TRIP-Matrix-Composite under Cold Working Conditions. *Mater. Sci. Appl.* **2014**, *5*, 812–822. [[CrossRef](#)]
49. Vahed, N. *Einfluss des Materialflusses auf die Verdichtung beim Sinterschmieden*; Umformtechnik: Verlag Meisenbach GmbH, Bamberg, Germany, 2014; pp. 2–11.

